Measurements of classical transport of fast ions

L. Zhao, W. W. Heidbrink, H. Boehmer, and R. McWilliams
Department of Physics and Astronomy, University of California, Irvine, California 92697

D. Leneman and S. Vincena
Department of Physics and Astronomy, University of California, Los Angeles, California 90095

(Received 26 January 2005; accepted 10 March 2005; published online 5 May 2005)

To study the fast-ion transport in a well controlled background plasma, a 3-cm diameter rf ion gun launches a pulsed, ~300 eV ribbon shaped argon ion beam parallel to or at 15° to the magnetic field in the Large Plasma Device (LAPD) [W. Gekelman, H. Pfister, Z. Lucky, J. Bamber, D. Leneman, and J. Maggs, Rev. Sci. Instrum. **62**, 2875 (1991)] at UCLA. The parallel energy of the beam is measured by a two-grid energy analyzer at two axial locations ($z=0.32$ m and $z=6.4$ m) from the ion gun in LAPD. The calculated ion beam slowing-down time is consistent to within 10% with the prediction of classical Coulomb collision theory using the LAPD plasma parameters measured by a Langmuir probe. To measure cross-field transport, the beam is launched at 15° to the magnetic field. The beam then is focused periodically by the magnetic field to avoid geometrical spreading. The radial beam profile measurements are performed at different axial locations where the ion beam is periodically focused. The measured cross-field transport is in agreement to within 15% with the analytical classical collision theory and the solution to the Fokker–Planck kinetic equation. Collisions with neutrals have a negligible effect on the beam transport measurement but do attenuate the beam current. © *2005 American Institute of Physics*.
[DOI: 10.1063/1.1905863]

I. INTRODUCTION

Fast ions may have velocities v_b that are much larger than the thermal velocity of the background plasma ions v_i but much less than the thermal velocity of the background plasma electrons v_e, i.e., $v_i \ll v_b \ll v_e$. In many natural and laboratory plasmas, the fast-ion density n_b is much less than the background plasma density, i.e., $n_b \ll n_e$. Thus, the fast-ion beam acts as a test beam that is decelerated and deflected due to multiple Coulomb collisions with the background ions and electrons. In a uniform plasma, this process is described by classical transport theory.[1–6]

Collisional transport of the energetic ions is a fundamental topic of plasma theory and experiments. In fusion devices and space plasmas, the deceleration rate of the fast-ion beam determines the heating rate and the energy transferred to ions or electrons from the beam. The collisional scattering impacts the flow driven by a beam, the particle transport to the loss cone, and the duration of resonant wave-particle interaction.

In classical Coulomb scattering theory, the impact parameter b is defined as the closest distance between two charged particles in the absence of Coulomb forces. For a test particle in a plasma, the cumulative impact parameter of many small-angle deflections has a cutoff at $b_{\max}=\lambda_D$ (Debye length). The Coulomb logarithm is defined as $\ln\Lambda = \ln(\lambda_D/b_0)$, where b_0 is 90°-scattering impact parameter. The formulas of $\ln\Lambda$ (λ_D and b_0 are different for different ions and electrons) are given in Ref. 2. Theoretically, the classical transport rates are proportional to the Coulomb logarithm. Recent theoretical papers have argued that modifications to classical Coulomb theory are required. A new cutoff[7] or the concept of collision strength[8] is introduced for small-angle scattering. The Coulomb logarithm is predicted to decrease by a factor of 2. The modified classical theory predicts reduced deceleration rates and cross-field transport.

The deceleration of fast ions has been measured in tokamak plasmas and agrees with the standard classical Fokker–Planck theory to within 10%.[9–14] Also the slowing-down of a barium ion beam with energy 0–40 eV was measured in a Q-machine in which the quiescent plasma ($T_e \approx 0.2$ eV) is confined by a uniform magnetic field.[15] The changes in velocity (due to beam slowing-down) agree with the predictions of the Fokker–Planck equation within error bars for different ions at different densities. E_{beam}/T_e is up to ~200 for the experiments in Ref. 15, but E_{beam}/T_e for the experiments that will be discussed in this article is ~1000–3000.

The velocity-space transport of test ions with velocity $|v_{\text{test}}/v_{\text{th}}| \leqslant 2$ (v_{th} is the thermal velocity of the background plasma ions) was measured in a fully ionized Q-machine plasma. The velocity-space convection coefficient (slowing-down) and parallel diffusion coefficient $D_{v_z v_z}$ were found to have the correct magnitude, and dependence on test-ion velocity and plasma density (which was varied by an order of magnitude) when compared to classical theory. Also the classical theory could predict the diffusion of the test particles distribution for up to 20% of the 90°-collision time in the long-time experiments.[16]

In classical transport theory, cross-field diffusion is caused by pitch-angle scattering in velocity space. Experimentally, accurate measurements of the spatial diffusion of the fast ions are rare.[9] The pitch-angle scattering rate in mirror machines can be of the same order of magnitude as classical predictions.[17] The result of an experiment measuring the cross-field transport of test ions with velocity $v_f < 2v_i$ in a

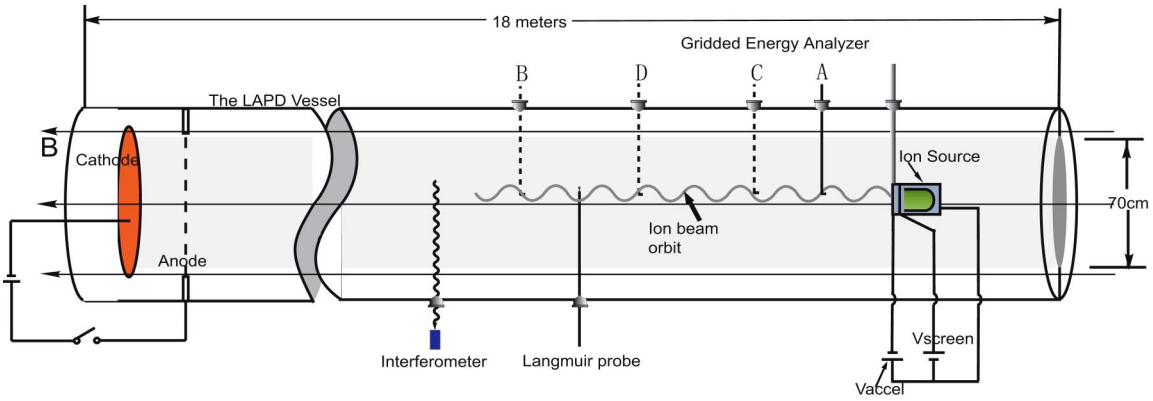

FIG. 1. (Color online). Schematic of the experimental setup. Plasma in the LAPD is generated by the cathode-anode discharge. A 3 cm rf ion gun is inserted from the top of the LAPD vessel. The 300 eV ion beam follows a helical orbit along the uniform magnetic field line. A Langmuir probe and an interferometer are used to measure the parameters of the background plasma. The energy analyzer can be placed at several positions (port *A*, *B*, *C* and *D* in the graph) downstream of the ion beam through radial, rotary ports built on the LAPD. The energy and spatial distribution are measured by the energy analyzer.

Q-machine agrees with the prediction of the modified Langevin equation.[18] Numerous measurements of the pitch-angle scattering rate in the tokamaks show rough agreement with the neoclassical theory,[9,19,20] but the uncertainties can be of order unity and lack quantitative comparisons. A more accurate measurement confirms the classical theory within uncertainties of $\leqslant 15\%$.[21] In magnetosphere plasmas, pitch-angle diffusion is important for driving trapped energetic particles into the atmospheric loss cone. Satellite observations in the outer magnetosphere find that the fluxes of energetic protons (energy $\sim$5–70 MeV) rise and decay on time scales $\sim$15 min due to the particle pitch-angle diffusion.[22]

This article describes experiments that measure accurately the deceleration and spatial diffusion of fast ions in a quiescent laboratory plasma, which is generated in the Large Plasma Device (LAPD) (Ref. 23) at UCLA. The large size of the LAPD and the excellent computer characterization ability are well suited for laboratory studies of fast-ion transport. The test-ion beam is an argon beam with energy 300–400 eV. A two-grid energy analyzer is the main diagnostic for this experiment (Sec. II). The measurements of the fast-ion slowing-down time and cross-field transport are discussed separately (Secs. III and IV). The comparison of the results with the classical Coulomb collision theory and the uncertainties of the experiments are also included in these sections. The collisions between the fast-ions and neutral particles only attenuate the beam current without affecting the transport of the ion beam (Sec. V). The experimental results agree with classical transport theory (Sec. VI).

II. EXPERIMENTAL SETUP

The diagram of the experiment is shown in Fig. 1. The plasma in the LAPD is generated by a negative dc discharge of the barium oxide coated cathode with respect to a mesh anode 60 cm from the cathode. The 5–10 ms discharge pulse is repeated at 1 Hz. The plasma column is 17 m in length and 50 cm in diameter. The argon gas is fed through the ion gun, so the background plasma is an argon plasma and the beam is a fast argon ion beam. The parameters of the LAPD plasma are measured by a Langmuir probe and an interferometer, which measures the integrated density along a line across the magnetic field.

A 3-cm diameter rf ion beam source[24] is modified to produce a pulsed ribbon shaped (3 cm$\times$0.5 cm) argon ion beam in the parallel direction or with 15° to the magnetic field in the LAPD. The energy of the beam is the sum of the screen grid bias, the plasma potential of background plasma, and the plasma potential of the plasma inside the ion source, which is dependent on the rf power and the gas flow rate. The density of the ion beam is about 1.0×10^8 cm^{-3}, which is only 1% of the background plasma density. The beam current is large enough for the detection by an energy analyzer as far as 6.4 m away from the ion gun. Typical beam current density is about $1\sim3$ mA/cm^2. Also the beam has small divergence and small energy spread, as required for the spatial diffusion measurements. A detailed description of the rf ion source can be found in Ref. 24.

The two-grid energy analyzer is installed in different ports (*A*, *B*, *C*, and *D* in Fig. 1) on the LAPD vessel to measure the beam energy or scan over a plane to measure the beam width. Its small size (0.46 cm diameter) and good energy resolution make accurate measurements of the beam slowing down and diffusion possible (see Fig. 2). The resolution of the energy analyzer is calibrated by laser-induced fluorescence (LIF).[24] The first (outer) grid of the energy analyzer is grounded to the vessel potential. The second grid is biased 60 V negatively to the vessel. A variable dc bias box is connected to the collector and the data acquisition system. It not only provides the programable sweeping voltage to the collector but also measures the voltage and current signals using isolation amplifiers.

The LAPD afterglow plasma becomes relatively quiescent (density fluctuation $\delta n/n\leqslant1\%$) 5–10 ms after the discharge is terminated. During the afterglow the plasma temperature falls rapidly while the density continues to decay slowly [Fig. 3(a)]. The parameters of the plasma were determined by Langmuir probe measurements in the afterglow phase. To get a full *I-V* trace, the voltage of the Langmuir probe ramps from −25 to 10 V in about 0.2 ms. Electron

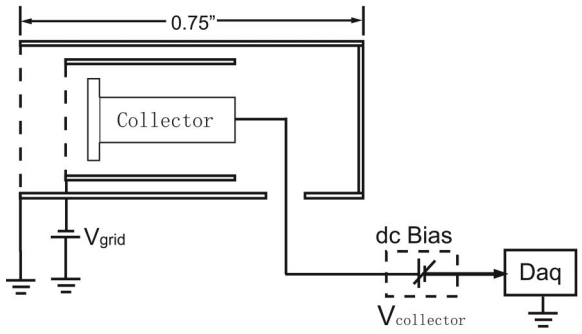

FIG. 2. Diagram of a two-grid energy analyzer. The diameter of the collector is 0.46 cm. The outer grid is connected to the metal housing, which is grounded at the LAPD vessel. The inner grid is biased at −60 V to the outer grid to repel the plasma electrons. The collector is connected to a variable dc power supply which can sweep from 0 to 1000 V.

temperature T_e [Fig. 3(c)] is derived by fitting the transition region of the *I-V* trace using $\exp(eV/T_e)$. The plasma density is calculated from the ion saturation current. The absolute calibration is obtained by calculating the line integral of the probe data and normalizing to the more accurate interferometer measurements. The plasma temperature and density have $<30\%$ variation in the region where the ion beam propagates. The central T_e and n_e of the background plasma (line averaged over 40 cm) is used in the theoretical predictions of the fast-ion transport.

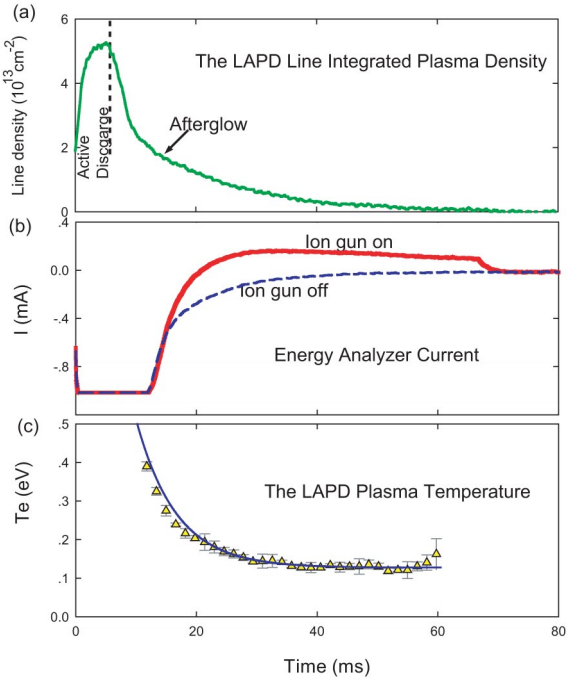

FIG. 3. (Color online). Time evolution of the LAPD plasma and the current measured by the energy analyzer. (a) Plasma line density measured by the interferometer. (b) Beam current signals measured by the energy analyzer when rf is on or off. The collector is biased at +60 V to the LAPD vessel. Between 0 and 20 ms, a large electron current is induced by the active discharge into the energy analyzer system which has a time constant of about 2 ms. (c) The electron temperature of the LAPD plasma measured by Langmuir probe. The solid line is the smoothed temperature.

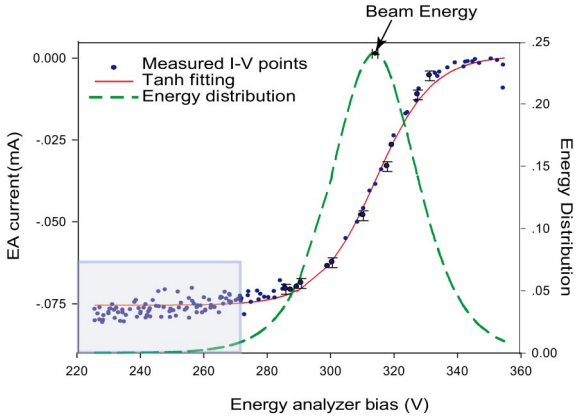

FIG. 4. (Color online). Hyperbolic tanh curve fitting of the *I-V* trace to find beam energy. The dots are the measured *I-V* characteristic points. The solid curve (the energy distribution) is the *I-V* trace fitted by tanh function. In the shaded area, the fit is not very good but hardly affects the energy distribution. The differential of the *I-V* trace, the dashed line, is the measured energy distribution. The beam energy is defined as the peak of the distribution; the error bar represents the sensitivity of the beam energy to variations in fitting parameters.

By modulating the amplitude of the rf power, the ion source was turned on for 50 ms during each LAPD pulse. Figure 3(b) shows the typical current signal measured by the energy analyzer when the rf power of the ion source is on and off. The fast-ion transport is measured during 20–70 ms to avoid the active discharge phase. The net beam current is the difference between the two signals.

III. SLOWING-DOWN OF THE FAST-ION BEAM

A. Description of the experiment

In experiments measuring the beam slowing-down, the ion beam is launched parallel to the magnetic field in the LAPD. The screen grid of the rf ion beam source is biased at 150 V dc. The beam energy at this bias is about 300 eV due to the source plasma potential, as mentioned above.

The energy analyzer is first used to find the beam center, the point of highest beam density. At that point, the beam energy distribution is determined. The bias control box connected to the collector of the energy analyzer (see Fig. 2) can provide 0–1000 V variable dc bias but with a slow time response of about 1 s. During the energy scan, the collector bias is varied from 250 to 350 V over many plasma pulses at a different frequency to avoid possible systematic errors. Here we assume the bias voltage is constant in each 80-ms data collecting window, which is much shorter than its response time. The input dc bias voltage and the output current are digitized simultaneously in order to get a full *I-V* trace. The valid *I-V* points[25] are shown as the dots in Fig. 4.

The derivative of the *I-V* trace is related to the energy distribution of the ion beam.[26] The peak of the energy distribution agrees well with independent LIF measurements, but the energy distribution is broader for the energy analyzer due to instrumental effects.[15] The beam energy is defined as the peak of the energy distribution (Fig. 4). Fitting the *I-V* trace with a hyperbolic tanh function accurately determines the peak energy with minimal sensitivity to errors in the data.

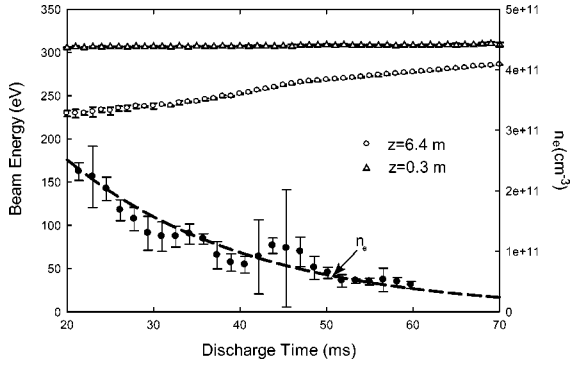

FIG. 5. Measured beam energy vs time at two different axial locations. The density of the LAPD plasma is also plotted (the solid dots and the dashed smooth curve). Some error bars are smaller than the symbol size. Chamber pressure $P=2.3\times10^{-5}$ Torr, argon gas flow is 1.3 SCCM (SCCM denotes cubic centimeter per minute at STP) the screen grid bias of the ion gun $V_{\text{screen}}=150$ V, magnetic field $B=1.0$ kG, and ion gun is parallel to the field line.

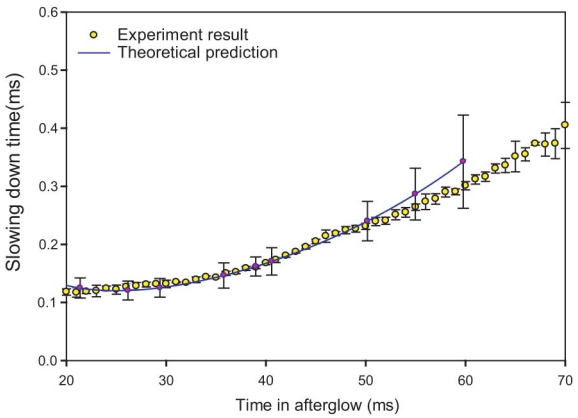

FIG. 6. (Color online). Fast-ion beam slowing-down time. The dots are calculated from the experimental results. The smooth line is the prediction by the classical Coulomb collision theory. The large error bars in the late afterglow phase are mainly due to the uncertainty in the electron density measurements.

(Due to neutral collisions, the beam contains a small, low-energy component that causes deviation from the tanh fit at low energy.)

The energy scans are conducted at two axial locations, $z=0.3$ m (at point *A* in Fig. 1) and $z=6.4$ m (point *D*) from the beam. The measured beam energy is lower far from the source than near the source because the fast ions decelerate as they traverse the plasma (Fig. 5). When the energy analyzer is at $z_1=0.3$ m, the energy is nearly a constant because the slowing-down effect is small in such a small distance. But when the energy analyzer is at $z_2=6.4$ m, the beam is decelerated more (lower beam energy) in the early afterglow time when the LAPD plasma has higher density.

B. Beam energy loss time

The beam slowing-down time τ_s is derived by $dv_b/dt=-(v_b/\tau_s)$ or in the integral form $v_b=v_{b0}\exp(-t/\tau_s)$, where v_b represents the velocity of the fast ions and v_{b0} is a constant. Assuming E_1 is the beam energy measured at axial position z_1 when $t=t_1$ and E_2 is the beam energy measured at axial position z_2 when $t=t_2$, we have

$$E_1=\tfrac{1}{2}M_b v_1^2=\tfrac{1}{2}M_b v_{b0}^2\exp(-2t_1/\tau_s), \tag{1}$$

$$E_2=\tfrac{1}{2}M_b v_2^2=\tfrac{1}{2}M_b v_{b0}^2\exp(-2t_2/\tau_s), \tag{2}$$

and

$$\Delta z=z_2-z_1=\int_{t1}^{t2}v_b dt=\int_{t1}^{t2}v_{b0}e^{-t/\tau_s}dt$$
$$=\tau_s(v_{b0}e^{-t_1/\tau_s}-v_{b0}e^{-t_2/\tau_s}). \tag{3}$$

Therefore, the experimental slowing-down time can be solved from Eq. (1)–(3),

$$\tau_s=\frac{\Delta z M_b^{1/2}}{\sqrt{2}(\sqrt{E_1}-\sqrt{E_2})}. \tag{4}$$

When the fast ion is slowed down equally due to electron collisions and ion collisions, the energy of the fast ion is defined as the *critical energy* $E_{b,\text{crit}}$.[27] Since the fast-ion energy is much larger than the critical energy $E_{b,\text{crit}}$, which is about $51T_e$ for a singly ionized argon beam in a singly ionized argon plasma, theoretically the collisions with electrons dominate the slowing-down process of the test-ion beam. But electron collisions barely deflect the fast ions from their original direction of motion. According to the conventional Coulomb collision theory, if $v_b\ll v_e$, the beam ion slowing-down rate ν_s can be calculated by[2]

$$\nu_s=2\left(1+\frac{M_b}{m_e}\right)\Psi(x)\nu_0\approx 4\times10^{-11}T_e^{-(3/2)}n_e\ln\Lambda_{ie}, \tag{5}$$

where $\nu_0=(4\pi e^4 n_e\ln\Lambda)/M_b^2v_b^3$, $x=(m_e v_b^2)/2kT_e$, $\Psi(x)$ is the error function, and $\ln\Lambda_{ie}$ is Coulomb logarithm. $\ln\Lambda_{ie}=23-\ln(n_e^{1/2}T_e^{-(3/2)})$ for $T_e\ll10$ eV, T_e is in eV and all other units are CGS.

The theoretical slowing-down time, $\tau_s=1/\nu_s$, is a function of the background plasma parameters T_e and n_e, which have been measured with a microwave-interferometer calibrated Langmuir probe. Using Eqs. (4) and (5), the theoretical and experimental slowing-down time is computed and shown in Fig. 6. The measured experimental slowing-down time is in agreement with the theoretical prediction within the error bars (which are large in the late afterglow phase where the plasma density measurement has larger uncertainty). Since the plasma temperature T_e drops quickly and is nearly a constant after 20 ms in the afterglow, the slowing-down time is a linear function of the inverse of n_e [Eq. (5)]. As is shown in Fig. 6, the slowing-down time is shorter in the early afterglow than in the late afterglow. In other words, the fast-ion beam decelerates more when the plasma density is higher in the early afterglow.

The random error associated with the tanh fitting in the energy measurement (Fig. 4) is less than 5%. The theoretical predictions have larger uncertainties (10%–30%) associated with the errors in the Langmuir probe measurements of T_e and n_e. In the late afterglow phase, the plasma density measurements could have uncertainty of 40% (see Fig. 6) due to the difficulty of measuring such low density. There are also

several possible systematic errors. It has been mentioned that the absolute plasma density is calibrated by the line integrated density measured by an interferometer. Langmuir probe measurement is performed along a 50-cm horizontal line in the middle of the plasma column, but the interferometer measures the line integrated plasma density over the whole diameter of the plasma column. By ignoring the edge of the plasma, the calibrated n_e could be 10% larger than the actual plasma density. Also, the interferometer measurement is closer to the cathode than the region where the fast ions are measured. To calculate the slowing-down, the T_e and n_e data are averaged over a 40-cm line across the center of the LAPD plasma. The spatial averaging of T_e and n_e could be different from what the actual ion beam sees in the plasma. The interpretation of Langmuir probe data also has possible systematic errors. Finally, if the source is not perfectly parallel to the magnetic field, the ion beam path is longer. Estimates indicate that these systematic errors are smaller than the random uncertainty of the theoretical prediction.

To quantify the uncertainties in the beam slowing-down measurement, let χ_i=experimental τ_s/theoretical τ_s and its error $\sigma_i/\chi_i=\sqrt{(\sigma_{\text{expt}}/\tau_{s\ \text{expt}})^2+(\sigma_{\text{th}}/\tau_{s\ \text{th}})^2}$ at each measured point. The weighted average is $\overline{\chi}=\Sigma_i w_i\chi_i/\Sigma_i w_i$, where $w_i=1/\sigma_i^2$. Calculated over all the points measured in the experiment, $\overline{\chi}=94.4\%\pm7.4\%$. This shows the classical theory accurately describes the fast-ion beam deceleration process. The modified theory,[7] which doubles the theoretical slowing-down time and yields $\overline{\chi}=47.2\%\pm3.7\%$, does not fit the experimental results.

IV. FAST-ION CLASSICAL DIFFUSION

In the plasma physics literature, cross-field diffusion usually refers to radial transport of guiding centers. In our experiment, the fast ions only execute a few Larmor orbits prior to measurement, so it is conceptually simpler to examine the full helical Lorentz orbit than the guiding-center orbit. Pitch-angle scattering events shrink or expand the diameter of the helical orbit. Radial spreading of the beam is caused primarily by perpendicular spreading of the beam in velocity space.

A second distinction from standard transport theory is that, in standard theory, ion-ion collisions (like-particle collisions) do not lead to any net change in flux. However, in this experiment, the high-energy ions are test particles that are readily distinguished from the cold thermal ions, so ion-ion collisions are observable. Although these ion-ion collisions are less frequent than collisions with electrons, they dominate the pitch-angle scattering rate because collisions with relatively light electrons decelerate fast ions without deflecting them in angle.

A. Arrangement of the experiment

The experimental setup and a helical beam trajectory are illustrated in Fig. 1. The energy analyzer, which is biased at 60 V relative to the vessel, can effectively detect the fast-ion beam and measure the beam profile by scanning over a plane across the field line. To make the spatial diffusion more visible, it is important to turn the ion source at an angle to the magnetic field to focus the beam periodically to avoid geometrical effects due to initial beam divergence.

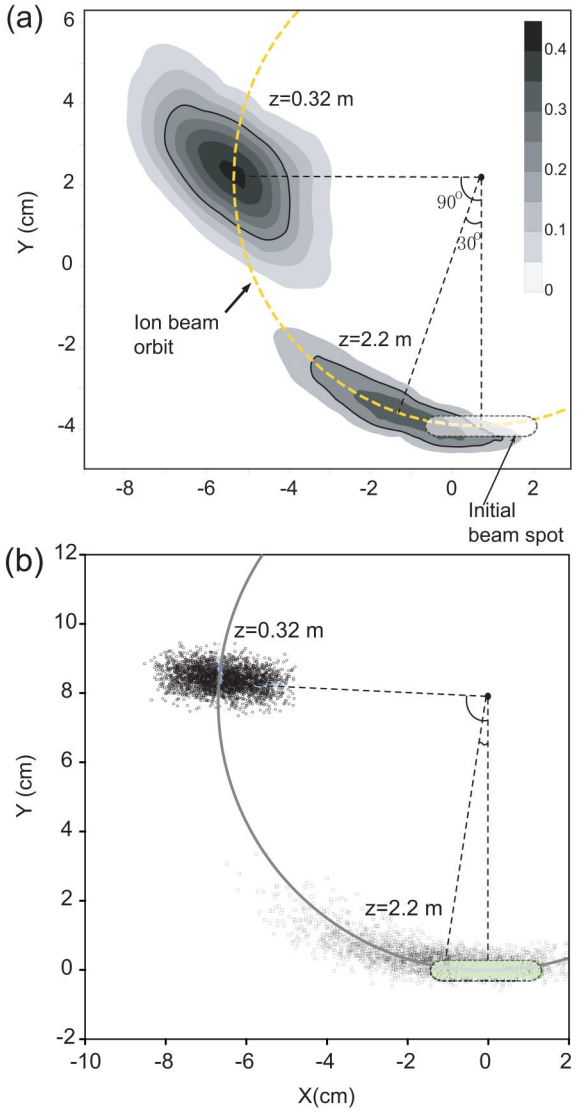

FIG. 7. (Color online). Geometrical effects of the beam contours. (a) Contours measured at 60 ms in the afterglow (when collisional diffusion is small). The initial beam spot is formed by the ion beam passing through a thin slit aperture. The plasma and beam parameters of these measurements are magnetic field $B=1$ kG, flow rate=1.3 SCCM, $V_{\text{screen}}=250$ V, and 20° beam pitch angle. (b) The beam spots predicted by the Monte Carlo ion orbit simulation program on each plane under the same conditions as (a).

If the parameters of the experiment are not carefully arranged, the geometrical effects can obscure the spatial diffusion, which is relatively small. For example, Fig. 7(a) shows two contours measured at different axial locations when geometrical effects are significant. The contour measured at $z=0.3$ m from the source is much wider than the one measured at $z=2.2$ m, which is supposed to spread more due to the longer scattering path.

A Monte Carlo fast-ion orbit simulation program[25] is used to explore the appropriate parameters for the fast-ion transport experiments. In the program, a fast-ion beam is launched into a plasma at a certain angle with respect to the magnetic field. The ion gyro-orbit, which is modified by col-

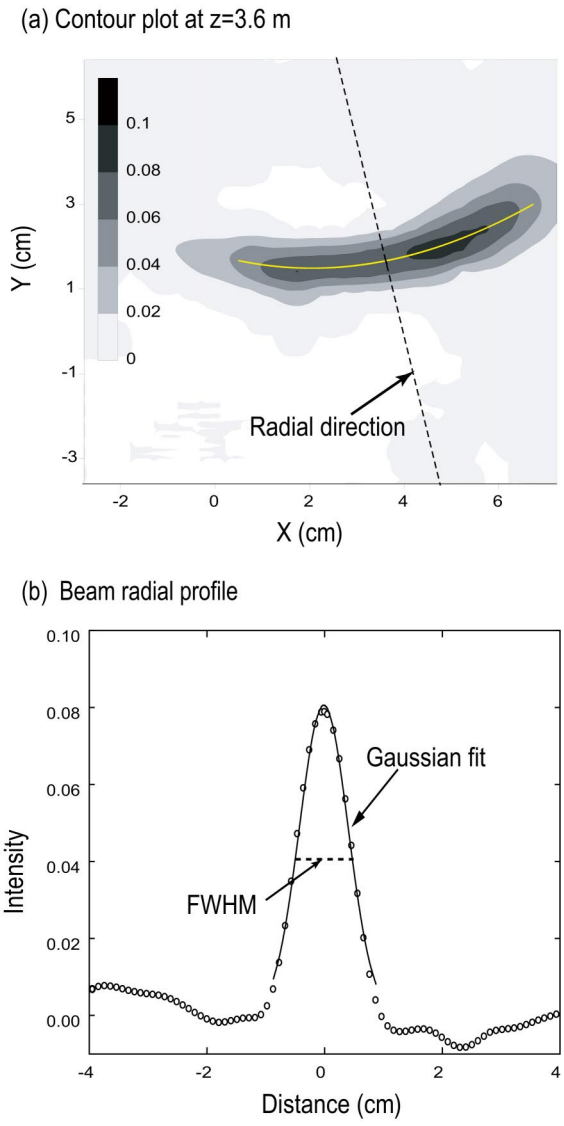

FIG. 8. (Color online). Illustration of the Gaussian radial profile. (a) Measured beam contour at $z=3.6$ m away from the source 40 ms in the afterglow. The dashed line is the radial direction. (b) Beam radial profile and its Gaussian fit. Beam width is defined as the FWHM of the radial profile.

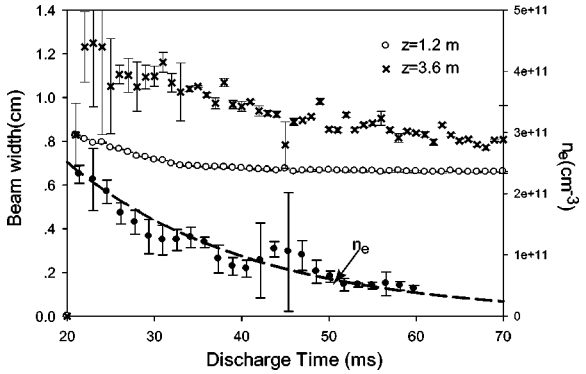

FIG. 9. Beam width vs discharge time of the LAPD plasma. Beam widths are measured by energy analyzer scanning over a plane perpendicular to the magnetic field at two different axial locations from the source. The LAPD plasma density n_e is also plotted (the solid dots and the dashed smooth curve). Experimental parameters are the LAPD chamber pressure $P=2.3\times10^{-5}$Torr, argon gas flow is 1.3 SCCM, magnetic field $B=0.85$ kG; ion source is at 15° to the field line; $V_{\text{screen}}=220$ V. Error bars for the $z=1.2$ m are smaller than the symbol size.

lisions with the background plasma ions and neutrals, is followed and measured at several cross sections downstream. If we use the parameters in Fig. 7(a), the same geometrical effects will show up again in the result of the simulation program. Evidently the beam contour with the gyrophase close to $2n\pi$ has less orbital geometrical effects (see Figs. 7(a) and 7(b) when $z=2.2$ m).

According to the above discussions, to minimize the geometrical effects in the experimental results that follow, the beam energy, beam orientation, and magnetic field need to be adjusted so that the gyrophase of the beam spot is $2n\pi$ at the port where the energy analyzer measures the spatial diffusion. After the adjustment of the operation parameters (to what are used in Fig. 9), the helical beam orbit finishes one revolution during each four-port period (distance is 1.2 m) on the LAPD. The energy analyzer was put at point $C(z=1.2$ m) or $D(z=3.6$ m) in Fig. 1 to scan the beam spot over a plane across the magnetic field. A typical beam contour spot is shown in Fig. 8(a). It is in an "arc" shape because the ion beam tends to spread along the gyro-orbit due to the beam energy spread. When the gyrophase of the beam spot is close to $2n\pi$, the measured beam spot should distribute along the bottom of the gyro-orbit.

To quantify the spatial spreading, a smooth arc line is fit to the beam spot. The perpendicular to this arc [dashed line in Fig. 8(a)] is defined as the radial direction. The radial profile along this line, plotted in Fig. 8(b), is very close to a Gaussian distribution. Gaussian spreading is consistent with diffusive spreading, as expected classically. The width of the beam is the weighted average full width at half maximum (FWHM) of the radial profiles along the beam arc. The weight is the goodness (χ^2) of the Gaussian fitting.

The beam width measured at two different distances from the source is plotted in Fig. 9 as a function of the time in the afterglow. The fast-ion beam has a larger width far from the source ($z=3.6$ m) than close to the source ($z=1.2$ m) due to more collisions with the plasma. Also, since the density of the LAPD plasma is higher at early times in the afterglow resulting in more Coulomb collisions, the beam widths and beam spreading are larger at the early time than at the late time in the afterglow as shown in Fig. 9.

B. Diffusion coefficient derived from the experiment results

The ion beam profile consists of an initial beam spot size $\langle(\Delta r_0)^2\rangle$ and a diffusive spread $\langle(\Delta r)^2\rangle$. Therefore, the total radial beam spread should be $[\langle(\Delta r_0)^2\rangle+\langle(\Delta r)^2\rangle]$, and the total beam radial distribution should be

$$P(r) \propto e^{[(r-r_0)^2]/2[\langle(\Delta r_0)^2\rangle+\langle(\Delta r)^2\rangle]}. \tag{6}$$

As stated before (Fig. 9), the beam width W_{beam} is defined as the FWHM of the beam radial profile $P(r)$. Thus,

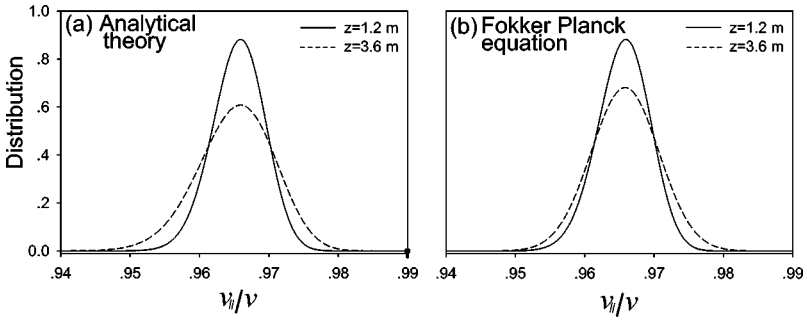

FIG. 10. Beam angular spread in velocity space. (a) Predicted by the analytical theory. (b) Solution to the Fokker–Planck equation.

$$W_{\text{beam}}^2(t) = 8\ln 2[\langle(\Delta r_0)^2\rangle + \langle(\Delta r)^2\rangle] = 5.545[\langle(\Delta r_0)^2\rangle + 2D_\perp t], \tag{7}$$

where $D_\perp = \langle(\Delta r)^2\rangle/(2t)$. This is very similar to the result given in Ref. 18.

Let W_1 and W_2 represent the beam width measured at two axial positions, $z_1 = 1.2$ m and $z_2 = 3.6$ m in this experiment. According to Eq. (7),

$$W_1^2 = 5.545\langle(\Delta r_0)^2\rangle + 11.09D_\perp t_1$$

and

$$W_2^2 = 5.545\langle(\Delta r_0)^2\rangle + 11.09D_\perp t_2,$$

where $t = (\Delta z)/v_\parallel$. Then the experimental radial diffusion coefficient is

$$D_{\perp\text{expt}} = \frac{W_2^2 - W_1^2}{11.09(t_2 - t_1)} = \frac{W_2^2 - W_1^2}{11.09\Delta t}. \tag{8}$$

Since the beam widths are measured in the experiment, the spatial diffusion coefficient is decided by Eq. (8).

C. Analytical pitch-angle scattering theory

Consider a fast-ion beam that is launched into the LAPD plasma with an initial pitch angle θ with respect to the direction of the magnetic field. Due to the Coulomb collisions, the ion velocity is scattered around the initial velocity $\overline{v}$. Assume v is the beam velocity after the collision, φ is the angle between v and $\overline{v}$, $\varphi \ll 1$, α is an azimuthal angle of v around $\overline{v}$, $0 \leqslant \alpha < 2\pi$. According to the classical Coulomb collision theory, the pitch-angle scattering rate ν_{PAS} is defined as[3] $\langle(\Delta v_\perp)^2\rangle/v^2 = \nu_{\text{PAS}}t$. With $\Delta v_\perp = (v - \overline{v})_\perp = v\sin\varphi \approx v\varphi$, the spread of φ is $\langle\varphi^2\rangle \approx \nu_{\text{PAS}}t$ approximately. In the LAPD coordinates, the perpendicular velocity component is

$$v_\perp \approx \overline{v}\sin\theta + v\varphi\cos\alpha\cos\theta, \tag{9}$$

which is derived by using the coordinate conversion and the approximation of $\varphi \ll 1$.

Since the new gyroradius of the fast-ion beam is $r = v_\perp/\Omega$ and the initial gyroradius is $\overline{r} = \overline{v}_\perp/\Omega = (\overline{v}\sin\theta)/\Omega$, where Ω is the gyrofrequency [$\Omega = (eB)/M$], the gyro-orbit changes by

$$\Delta r = r - \overline{r} = \frac{v_\perp - \overline{v}\sin\theta}{\Omega} = \frac{v\varphi\cos\alpha\cos\theta}{\Omega} \tag{10}$$

(using Eq. (9)]. Then the spatial spreading in radial direction is

$$\langle(\Delta r)^2\rangle = \frac{v^2\cos^2\theta}{2\Omega^2}\langle\varphi^2\rangle \approx \frac{v^2\cos^2\theta}{2\Omega^2}v_{\text{PAS}}t, \tag{11}$$

using $\langle(\cos\alpha)^2\rangle = \frac{1}{2}$ and $\langle\varphi^2\rangle \approx \nu_{\text{PAS}}t$. Here we assume the fast-ion energy spreading due to Coulomb collisions is small ($v^2 \sim$ constant) compared with pitch-angle spreading. The analytical form of radial diffusion coefficient $D_\perp$ is

$$D_{\perp\text{theor}} = \frac{\langle(\Delta r)^2\rangle}{2t} = \frac{v^2\cos^2\theta}{4\Omega^2}\nu_{\text{PAS}}, \tag{12}$$

where $\nu_{\text{PAS}} \approx 2.85\times10^{-8}n_iE_b^{3/2}\ln\Lambda_{ii}$ (for $v_i \ll v_b$ in Ref. 2).

D. Solution to the Fokker–Planck kinetic equation

The velocity-space transport of the energetic test beam can be accurately described by the Fokker–Planck kinetic equation theoretically. With the approximation of small beam deceleration $|(E_b - E_{b0})/E_{b0}| \ll 1$ and small pitch angle $|\xi - 1| \ll 1 (\xi = \cos\theta)$, the distribution function of the ion beam is expanded in Legendre polynomials $P_l(\xi)$; $f_b = \Sigma a_l(v,t)P_l(\xi)$. The solution to the kinetic equation for $a_l(v,t)$ is given by Goldston[28] for an ion beam that is described by a Green's function. Using the beam spreading measured at $z_1 = 1.2$ m as the initial beam, the predicted beam angular spreading at $z_2 = 3.6$ m is calculated by a computer program based on Goldston's solution (Fig. 10). Since the radial spreading is linear with the angular spreading [see Eq. (11)], the angular distribution in velocity space can be directly converted to the spatial distribution with the convolution with the initial beam distribution. The spatial diffusion coefficient is derived from the FWHM of the spatial distribution.

E. Comparison of theory with experiment

The measured spatial diffusion is compared with the theoretical prediction and the solution of the kinetic equation in Fig. 11. They are found to be consistent. Since fast-ion spatial diffusion is approximately linearly proportional to the plasma density n_i [see Eq. (12)], larger beam spreading in the early afterglow is seen in Figs. 9 and 11. In the early afterglow, the beam width measurement far from the source ($z = 3.6$ m) has large uncertainty because there are more off-orbit low-energy ions due to larger deceleration.

The random uncertainty of the beam spreading measurements is less than 10% except in the early afterglow phase between 20 and 30 ms (Fig. 9). The uncertainty of the theoretical prediction is mainly from the plasma density measure-

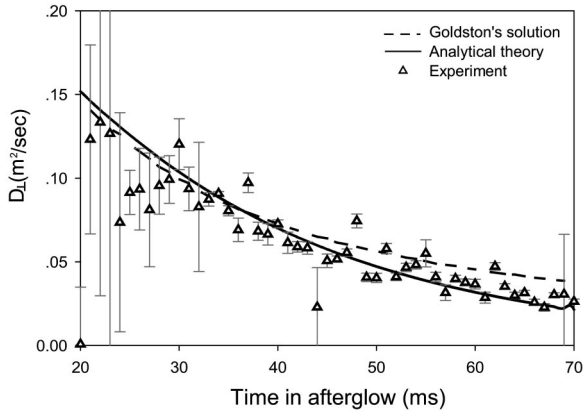

FIG. 11. Radial diffusion coefficient $D_\perp$ vs discharge time of the LAPD plasma. The solid line is predicted by analytical classic collision theory (see Sec. IV D). The dashed line is computed based on Goldston's solution to the Fokker–Planck kinetic equation. The triangle dots are derived from the beam widths measured from two different distances from the source.

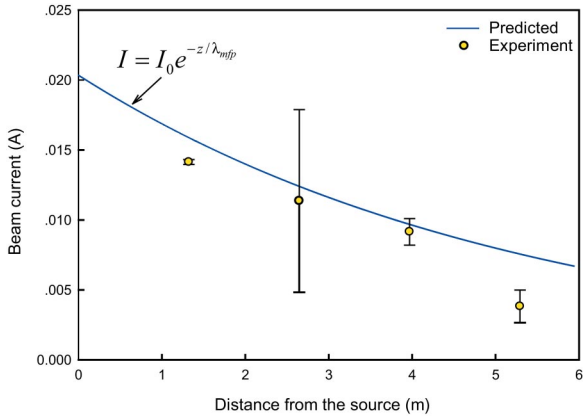

FIG. 12. (Color online). Fast-ion beam attenuation. The dots are total beam current measured at different distances from the ion source, which is at 15° to the magnetic field. The solid line is predicted by $I=I_0\exp(-z/\lambda_{\mathrm{mfp}})$, where the mean free path of charge exchange for argon ion with argon neutral
$\lambda_{\mathrm{mfp}}=5.3$ m (when $P=2.3\times10^{-5}$ Torr and beam energy is about 300 eV).

ment which is discussed in Sec. III B. The solution to the kinetic equation is sensitive to the divergence of the beam. To match the beam spot measured at $z_1=1.2$ m, the source divergence is approximately set as 3°, which is much smaller than the common rf ion source divergence ~10°.[29] The systematic errors come from several places. The angle of the ion beam source to the magnetic field could deviate 1° or 2° from the expected 15°. The gyrophases of the ion beam contours are not exactly the same as the initial beam spot. As a result, the geometrical effect could produce some systematic uncertainties. The magnetic field measurement has 3% uncertainty. Overall, the systematic uncertainty should be comparable to the random uncertainty.

To quantify the results, we use the same method as for the beam deceleration measurement. Here, $\chi_i=(\text{experimental } D_\perp)/\text{theoretical } D_\perp$ and its error $\sigma_i/\chi_i=\sqrt{(\sigma_{\mathrm{expt}}/D_{\perp\mathrm{expt}})^2+(\sigma_{\mathrm{th}}/D_{\perp\mathrm{th}})^2}$ at each point. The weighted average $\overline{\chi}$ is calculated to be $89\%\pm15\%$. If the modified theory[7] is applied, $\overline{\chi}$ would be $175\%\pm30\%$. Obviously, the standard classical transport theory is a better description of the spatial spreading caused by pitch-angle scattering of the fast ions.

Coulomb collisions not only decelerate and deflect the beam, but also cause a spread in beam energy. Energy diffusion in this experiment will cause additional spreading of the beam in gyroangle (along the arc in Fig. 8). Classically, energy diffusion is very small for a fast-ion beam that slows down primarily on electrons (<0.1 eV). Changes of this magnitude are much smaller than the ~10 eV energy spread[24] of the source and are undetectable experimentally. The experimental observations are consistent with this expectation. Experimentally, the arc length changes <10% during the afterglow.

V. COLLISIONS WITH NEUTRALS

It is necessary to mention the effects of the collisions between the fast ions and the neutral particles in the LAPD. The fast ion becomes a fast neutral by charge exchange with a background neutral particle, while the neutral particle becomes a slow ion (energy less than 60 eV). Neither the fast neutral nor the slow ion is collected by the energy analyzer. Thus, the fast beam ion is "lost" in these inelastic charge-exchange collisions. The measurements of the beam energy and spreading are unaffected, but the beam current attenuates as $I=I_0\exp[-(z/\lambda_{\mathrm{mfp}})]$ (Fig. 12), where z is the travel distance of the fast ion from the ion source and λ_{mfp} is the mean free path for charge exchange with neutral argon. In this experiment, $\lambda_{\mathrm{mfp}}\approx5.3$ m when $P=2.3\times10^{-5}$ Torr and beam energy is about 300 eV.[30]

During the time that argon fast ions move 2.5 m, only ~0.1% of the fast ions are lost due to radiative recombination.[31] This neutralization effect is negligible in the transport experiments or the beam attenuation experiments.

Another collisional process is the elastic scattering of the fast ions by the neutral particles. The mean free path of ion-neutral collision is about 8.0 m in this experiment, more than three times of the distance (2.4 m) a fast ion travels. When elastic scattering happens, the fast-ion velocity drops to $v_b'\approx v_b\cos\theta_d$, where θ_d is the deflection angle. For collisions of argon ions with argon neutrals, small-angle elastic scattering has the largest cross section.[32] For example, the differential cross section for deflection angles <1.0° is at least an order of magnitude higher than the differential cross section for deflection angles >4°. Small-angle collisions can affect the profile width but simulations[25] indicate the effect is negligible for the measurements shown in Fig. 8. When the deflection angle is large, the fast ions cannot be detected (lost). Similar to inelastic collisions, large-angle elastic collisions attenuate the beam current (in Fig. 12, the measured beam current is always slightly below the inelastic neutral collision prediction). For both cases, the neutral elastic scattering does not significantly change the measured transport properties of the fast-ion beam.

VI. CONCLUSIONS

The fast-ion beam energy and its deceleration process have been measured in the quiescent LAPD afterglow plasma when the ion beam source was in the direction par-

allel with the uniform magnetic field. The ion beam deceleration is mainly due to the Coulomb drag by the thermal electrons. The measured energy loss time is in good agreement $(94.4\% \pm 7.4\%)$ with the standard theoretical prediction, but not the modified theory[7] which doubles the energy loss time.

The cross-field diffusion was measured when the ribbon shape ion beam was launched at 15° to the magnetic field. To minimize the geometrical effects, the energy analyzer was put at the position where the gyrophase of the ion beam orbit is the same as the initial beam spot. The cross-field spreading of the beam was observed by scanning over the different planes normal to the magnetic field. The measured diffusion coefficient is consistent within 15% with the classical Coulomb collision theory and the solution to the Fokker–Planck kinetic equation. The modified Coulomb collision theory,[7] which reduces the deceleration rate and scattering rate by a factor of 2, is inconsistent with the results of this experiment.

The charge-exchange and elastic scattering with the neutral particles do not have obvious effects on the transport of the fast-ion beam in this experiment, but the beam current decreases exponentially due to the loss of the fast ions caused by the collisions with the neutrals.

Compared with the experiments described in Refs. 15,16, the beam energy in this experiment is much higher ($\sim$300 eV), so the measurements of beam energy and deceleration have better accuracy (the quantified uncertainties $<10\%$). The experiments in Ref. 16 also measured parallel velocity diffusion and evolution of velocity distribution of test ions with energy $<4T_e$. However, the beam ions in the current experiment move much faster in the parallel direction and the fast-ion travel time is so short that the parallel velocity diffusion (energy diffusion) is not observed.

Although its energy is much lower, the beam in this experiment operates in the same physics regime as the energetic ions in high temperature magnetic fusion devices, i.e., $v_i \ll v_b \ll v_e$ and $r_e \ll r_i \ll r_b$ (r is the gyroradius). A large body of work[9] has established that tenuous populations of fast ions with energies between 10 KeV and 15 MeV decelerate classically (to within accuracies of $\sim$10%), as observed here with a $\sim$300 eV beam. In contrast, measurements of spatial diffusion are extremely challenging in fusion devices. The observed transport of dilute fast-ion populations is of the same order as the neoclassical diffusion rate but has not been determined accurately.[9] The measurements reported here confirm that classical fast-ion transport prevails in quiet plasmas and further supports the expectation that, if fast-ion driven instabilities can be avoided, MeV alpha particles will be well confined in burning fusion plasmas.

This experiment is a preliminary work for the planned studies of fast-ion transport caused by fluctuations and wave-particle interactions in the LAPD. The classical transport theory is confirmed by the experiment and sets a basic limit for the fast-ion beam spatial diffusion.

ACKNOWLEDGMENTS

The authors gratefully acknowledge the assistance of W. Gekelman, V Laul, D. Edrich, D. Liu, Y. Zhang, and D. Zimmerman. This work was supported by NSF/DOE.

[1] B. A. Trubnikov, *Review of Plasma Physics 1* (Consultants Bureau, New York, 1965).
[2] *NRL Plasma Formulary* (U.S. Naval Plasma Laboratory, Washington, DC, 2002), p. 31.
[3] L. Spitzer, *Physics of Fully Ionized Gases* (Interscience, New York, 1962), Chap. 5.
[4] N. Rostoker, Nucl. Fusion **1**, 101 (1961).
[5] N. Rostoker and M. N. Rosenbluth, Phys. Fluids **3**, 1 (1960).
[6] N. Rostoker, Phys. Fluids **7**, 479 (1964).
[7] D. Li, Nucl. Fusion **41**, 631 (2001).
[8] Y. Chang, Phys. Plasmas **10**, 4645 (2003).
[9] W. W. Heidbrink and G. J. Sadler, Nucl. Fusion **34**, 535 (1994), and references therein.
[10] K. Tobita, K. Tani, T. Nishitani, K. Nagashima, and Y. Kusama, Nucl. Fusion **34**, 1097 (1994).
[11] ITER Physics Expert Group on Energetic Particles, Heating, and Current Drive, Nucl. Fusion **39**, 2471 (1999), and references therein.
[12] F. V. Tchernychev, Y. Kusama, M. Nemoto, A. Morioka, K. Tobita, and S. Ishida, Plasma Phys. Controlled Fusion **41**, 1291 (1999).
[13] W. W. Heidbrink, M. Miah, and D. Darrow *et al.*, Nucl. Fusion **43**, 883 (2003).
[14] V. G. Kiptily, Yu. F. Baranov, and R. Barnsley *et al.*, Phys. Rev. Lett. **93**, 115001 (2004).
[15] D. Newsham, T. J. Ross, and N. Rynn, Phys. Plasmas **3**, 2824 (1996).
[16] J. Bowles, R. McWilliams, and N. Rynn, Phys. Plasmas **1**, 3814 (1994)
[17] J. R. Hiskes and A. H. Futch, Nucl. Fusion **14**, 116 (1974), and references therein.
[18] R. McWilliams and M. Okubo, Phys. Fluids **30**, 2849 (1987).
[19] V. A. Yavorskij, J. W. Edenstrasser, V. Y. Goloborod'ko, S. N. Reznik, and S. J. Zweben, Nucl. Fusion **38**, 1565 (1998).
[20] D. Testa and A. Gondhalekar, Nucl. Fusion **40**, 975 (2000).
[21] W. W. Heidbrink, Phys. Plasmas **9**, 28 (2002).
[22] M. Schulz and L. J. Lanzerotti, *Particle Diffusion in the Radiation Belts* (Springer, Berlin, 1974), p. 126.
[23] W. Gekelman, H. Pfister, Z. Lucky, J. Bamber, D. Leneman, and J. Maggs, Rev. Sci. Instrum. **62**, 2875 (1991).
[24] H. Boehmer, D. Edrich, W. W. Heidbrink, R. McWilliams, and L. Zhao, Rev. Sci. Instrum. **75**, 1013 (2004).
[25] L. Zhao, Ph.D. thesis, University of California, Irvine, 2005
[26] C. Böhm and J. Perrin, Rev. Sci. Instrum. **64**, 31 (1993).
[27] R. J. Goldston and P. H. Rutherford, *Introduction to Plasma Physics* (IOP, London, 1995), p. 239.
[28] R. J. Goldston, Nucl. Fusion **15**, 651 (1979).
[29] G. Aston, H. R. Kaufman, and P. J. Wilbur, AIAA J. **15**, 516 (1978).
[30] M. A. Lieberman and A. J. Lichtenberg, *Principles of Plasma Discharges and Materials Processing* (Wiley, New York, 1994), p. 78.
[31] C. Kenty, Phys. Rev. **32**, 624 (1928).
[32] W. Aberth and D. C. Lorents, Phys. Rev. **144**, 109 (1966).